AIP | Journal of Applied Physics

Nanosecond in situ transmission electron microscope studies of the reversible Ge2Sb2Te5 crystalline amorphous phase transformation

M. K. Santala, B. W. Reed, T. Topuria, S. Raoux, S. Meister et al.

Citation: J. Appl. Phys. **111**, 024309 (2012); doi: 10.1063/1.3678447
View online: http://dx.doi.org/10.1063/1.3678447
View Table of Contents: http://jap.aip.org/resource/1/JAPIAU/v111/i2
Published by the American Institute of Physics.

Nanosecond *in situ* transmission electron microscope studies of the reversible $Ge_2Sb_2Te_5$ crystalline $\Longleftrightarrow$ amorphous phase transformation

M. K. Santala,,[1,a)] B. W. Reed,,[1] T. Topuria,[2] S. Raoux,[3] S. Meister,[4] Y. Cui,[5] T. LaGrange,[1] G. H. Campbell,[1] and N. D. Browning[1,b)]
[1]*Condensed Matter and Materials Division, Lawrence Livermore National Laboratory, Livermore, California 94551, USA*
[2]*IBM Research Division, Almaden Research Center, San Jose, California 95120, USA*
[3]*IBM T. J. Watson Research Center, Yorktown Heights, New York 10598, USA*
[4]*Intel Corporation, Hillsboro, Oregon 97124, USA*
[5]*Department of Materials Science and Engineering, Stanford University, Stanford, California 94305, USA*

(Received 11 October 2011; accepted 14 December 2011; published online 25 January 2012)

Chalcogenide-based phase-change materials have wide use in optical recording media and are growing in importance for use in non-volatile electronic memory. For both applications, rapid switching between the amorphous and crystalline phases is necessary, and understanding the changes during rapidly driven phase transitions is of scientific and technological significance. Laser-induced crystallization and amorphization occur rapidly and changes in atomic structure, microstructure, and temperature are difficult to observe experimentally and determine computationally. We have used nanosecond-scale time-resolved diffraction with intense electron pulses to study $Ge_2Sb_2Te_5$ during laser crystallization. Using a unique and unconventional specimen geometry, cycling between the amorphous and crystalline phases was achieved, enabling *in situ* transmission electron microscope (TEM) study of both microstructural and crystallographic changes caused by repeated switching. Finite element analysis was used to simulate interactions of the laser with the nano-structured specimens and to model the rapidly changing specimen temperature. Such time-resolved experimental methods combined with simulation of experimentally inaccessible physical characteristics will be fundamental to advancing the understanding of rapidly driven phase transformations. © *2012 American Institute of Physics*. [doi:10.1063/1.3678447]

I. INTRODUCTION

Phase change materials have two properties that make them technologically important: (1) the amorphous and crystalline phases have distinctly different optical and electronic properties and (2) they may be switched between phases rapidly and repeatedly through the application of heat pulses.[1] Laser-induced formation of meta-stable cubic $Ge_2Sb_2Te_5$ from the amorphous phase occurs in ~10–100 ns.[2] Laser amorphization is even more rapid (<10 ns)[3] and requires a quench rate of $\sim 10^{10}$ K/s.[3,4] The dynamic changes in atomic structure and microstructure driven by the extremely rapid temperature changes induced by laser (or Joule) heating are difficult to probe with conventional scattering and imaging instrumentation, but the need for experimental methods resolving rapid changes in phase change materials is becoming more pressing as the time scales for the phase transformations are reduced (down to 0.4 and 2.5 ns for electrical current driven amorphization and crystallization, respectively[5]).

The present work shows how new time-resolved *in situ* techniques can reveal transformations invisible to conventional bulk and low-time-resolution characterization. There have been numerous efforts to experimentally study laser-driven phase transformations in phase change materials either through *in situ* x-ray diffraction (XRD)[6–8] and TEM[9–12] or by post-mortem examination of laser-annealed films.[4,13,14] Time-resolved microbeam XRD has been used for *in situ* investigation of optical recording media, but to study laser-driven transformations, data must be integrated over many crystallization events using a stroboscopic approach.[8] XRD techniques probe atomic structure but not the microstructural changes during the phase transformation. In contrast, TEM can probe both crystal structure and microstructural changes, but, to date, studies of laser-annealed phase change materials have been limited to post-mortem examination after *ex situ* laser exposure, such as the study of laser-annealed films with fluctuation TEM by Lee *et al.*[13]; of as-deposited, primed, and melt-quenched amorphous Ge-Sb-Te films by Naito *et al.*[14]; or of the examination of laser marks by Yamada *et al.*[4] *In situ* TEM studies have been limited to heating using either a hot stage,[9,10] electron beam heating,[11] or, more recently, electrically driven by μs current pulses.[12] Of these, only the current-induced transformations come close to driving the phase transformation at the relevant nanosecond time scales, and only they have achieved both crystallization and amorphization during *in situ* TEM. The ability to study melt-quenched amorphous materials *in situ* is important because it has been shown that as-deposited and melt-quenched amorphous materials differ substantially in structure and crystallization characteristics.[13] While conventional *in situ* TEM may

[a)]Author to whom correspondence should be addressed. Electronic mail: santala1@llnl.gov.
[b)]Present address: Chemical and Materials Sciences Division, Pacific Northwest National Laboratory, Richland, WA, USA.

be used to collect microstructural and crystallographic information from dynamic processes, the temporal resolution is limited to ~1 ms, orders of magnitude too slow to resolve transient processes *during* laser-induced phase transformations. However, these transformations may be probed on the relevant time scales using brief exposures to intense electron pulses.

Such an electron probe has been achieved through the modification of a conventional TEM that enables photoemission of electrons. The instrument, called the dynamic transmission electron microscope (DTEM), is a unique electron microscope using intense electron pulses to achieve nanosecond-scale time-resolved imaging and diffraction of irreversible processes in condensed phases. During a time-resolved experiment, a reaction is initiated in the specimen with a "pump" laser pulse. A second laser pulse, which is timed against the pump laser pulse in an operator-defined delay, strikes the DTEM cathode inducing a burst of $\sim 10^{10}$ photoemitted electrons in a 15-ns pulse. The duration of the electron pulse passing through the reacting specimen defines the temporal resolution of the experiment. The design, operation, and limitations of the DTEM have been described in detail in Ref. 15 and 16. It is a powerful tool for the study of dynamic events, such as phase transformations, as demonstrated in metals[17,18] and semiconductors,[19] and it is applied here to the study of $Ge_2Sb_2Te_5$.

II. TIME-RESOLVED EXPERIMENTS

A. Experimental procedures

DTEM was used to examine crystallization in as-deposited amorphous films of 30 nm $Ge_2Sb_2Te_5$ deposited on a Si support with a 20 nm amorphous SiN_x window and an 8 nm SiO_x capping layer to prevent oxidation (Fig. 1(a)). The composition of the Ge-Sb-Te was measured by applying Rutherford backscattering spectroscopy (RBS) to find the Ge to Sb+Te ratio and particle-induced x-ray emission spectroscopy (PIXE) to find the Sb to Te ratio. The composition was found to be 22.0 ± 0.5 at. % Ge, 28 ± 5 at. % Sb, 50 ± 5 at. % Te. The accuracy for separating Sb and Te is low because the elements are close in mass, so within the errors it is $Ge_2Sb_2Te_5$. The DTEM pump laser used to induce crystallization has a 1064 nm wavelength (λ), a 135 ± 5-μm $1/e^2$ diameter, and a 12-ns FWHM pulse duration. Crystallization was induced with 2.7 μJ pulses. Electron diffraction patterns generated from 15-ns electron pulses were recorded. The pump-probe experiments were repeated for time delays ranging from 0 ns (electron probe simultaneous with pump laser) to 2 μs.

B. Results and discussion

Rotationally averaged electron diffraction data for all time-resolved diffraction patterns collected from 0 ns to 2 μs are shown in Fig. 1(b). The maximum temperature attained is between the crystallization temperature (T_c) of 415 K and the melting temperature (T_m) of 889 K[4] because crystallization occurred with no evidence of melting. It may be inferred that the peak temperature is closer to T_m than T_c because a 50% increase in laser energy will result in complete melting and dewetting. The peaks of the metastable cubic phase begin to develop within 1 μs of the initiating laser pulse. Before, during, and after diffraction data are shown for the 300 ns and 1 μm delays in Figs. 1(c) and 1(d), respectively. No substantial change is apparent in the before and during data for the 300 ns delay, but development toward the crystalline diffraction pattern is clear by 1 μs (Fig. 1(d)). The

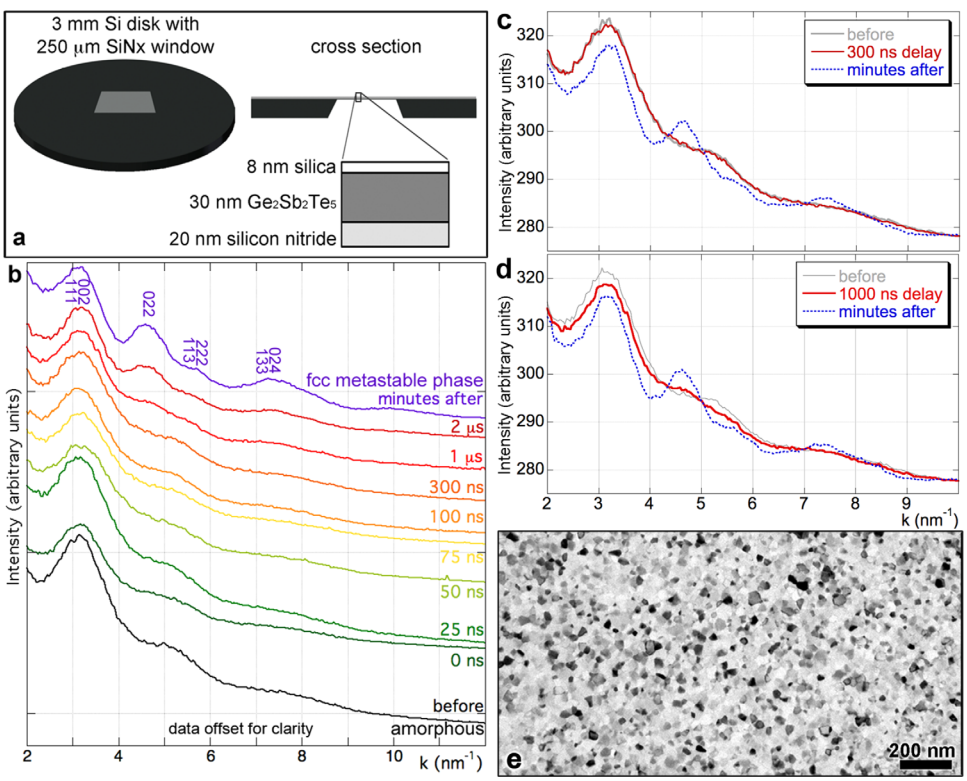

FIG. 1. (Color online) (a) Specimen schematic, (b) time-resolved, rotationally averaged electron diffraction intensity during laser-induced crystallization, (c) and (d) before, during, and after diffraction intensities for two time delays, and (e) film after crystallization, TEM image.

crystalline peaks are more prominent at 2 μs than 1 μs, indicating that nucleation and growth has progressed significantly in that time frame. By 2 μs, the diffraction data have all the features seen in the terminal diffraction pattern taken minutes after the pump laser struck the specimen. A conventional TEM image of a detail of the center of a laser-crystallized spot (Fig. 1(e)) shows a small (sub-micrometer) grain size as expected for nucleation-dominated crystallization, which is expected for $Ge_2Sb_2Te_5$.[20]

Crystallization did not occur in the 50–100 ns range anticipated for $Ge_2Sb_2Te_5$. Crystallization is affected by the duration and intensity of the laser pulse and may be slower for as-deposited than melt-quenched films, but in this case, a factor governing the relatively sluggish crystallization may also be the TEM specimen geometry. The specimen has a large, uniform electron-transparent area that was optimized for TEM experiments but that is different from the multilayered structure in optical recording media that have a metallic layer in close proximity to the phase change material. The difference in thermal transport properties may be anticipated to impact the kinetics of the crystallization. In addition to possibly affecting the kinetics of crystallization, when attempting to study the crystalline $\Rightarrow$ amorphous transition *in situ*, the electron transparent film is not in contact with an adequate thermal sink to quench into the amorphous state. Thin films deposited on electron transparent membranes, when melted, will re-crystallize rather than form an amorphous phase. This motivated the use of a less commonly used TEM specimen geometry, inspired by the geometry used for *in situ* nanoindentation studies,[21,22] where the specimen must be electron transparent and mechanically supported for indentation.

Optimally, a time-resolved, *in situ* experiment would be performed with a specimen geometry that induces quenching at a rate close to what occurs in optical memory devices; this would open an area of experimental investigation in repeatable, rapidly driven phase transformations. Hindering this is the stringent requirement that TEM specimens must be electron transparent. For a TEM operated in the conventional range of up to several hundred keV, sample thickness is limited to tens of nanometers. By implementing the geometry shown schematically and in a real cross section in Fig. 2, where the material at the tip of the wedge is electron transparent and in contact with a thermal sink, a higher cooling rate was achieved allowing *in situ*, laser-induced amorphization, as described in the following text.

III. SWITCHING EXPERIMENTS

A. Experimental procedures

A 50 nm $Ge_2Sb_2Te_5$ film supported on a 100 nm Mo layer and capped with 10 nm of amorphous alumina on a Si wedge was oriented in the electron and pump laser beams as shown in Fig. 2. RBS and PIXE results on a film deposited from the same target yield a composition of 18.5 ± 0.5 at. % Ge, 28.6 ± 5 at. % Sb, 52.9 ± 5 at. % Te; again the film is $Ge_2Sb_2Te_5$ within the error.

The pump laser ($\lambda = 1064$ nm, 135 ± 5-μm $1/e^2$ diameter, 12-ns FWHM) was used to induce the phase transformations in the deposited films as in the time-resolved experiments. The energy of the pump laser was varied to induce either crystallization through annealing or amorphization of crystalline film by a melt/quench process. Energies in the range of 8-23.2 μJ induced crystallization, and energies of 23.5-24 μJ were used to induce amorphization. TEM images and diffraction patterns were generated by a conventional, continuous electron beam by operating the DTEM in thermionic, rather than photoemission, mode.

B. Results and discussion

Diffraction patterns demonstrating the repeatable crystalline $\Leftrightarrow$ amorphous switching of $Ge_2Sb_2Te_5$ are shown in Fig. 3(a). The area used to generate the diffraction pattern is shown in Fig. 3(b) after a crystallizing and after an amorphizing pulse. This example of *in situ* TEM switching is currently a unique capability enabled by the *in situ* drive laser and the specialized specimen geometry. The same area could be tracked in both electron diffraction and imaging through multiple switching cycles. In this manner, it was demonstrated that the grains in the crystalline material take on different orientation relationships after each recrystallization event even after dozens of switching cycles. This indicates growth of grains in the melt from newly nucleated grains rather than rapid growth into the melt from adjacent crystalline material; this behavior is expected in materials that display nucleation-dominated crystallization.

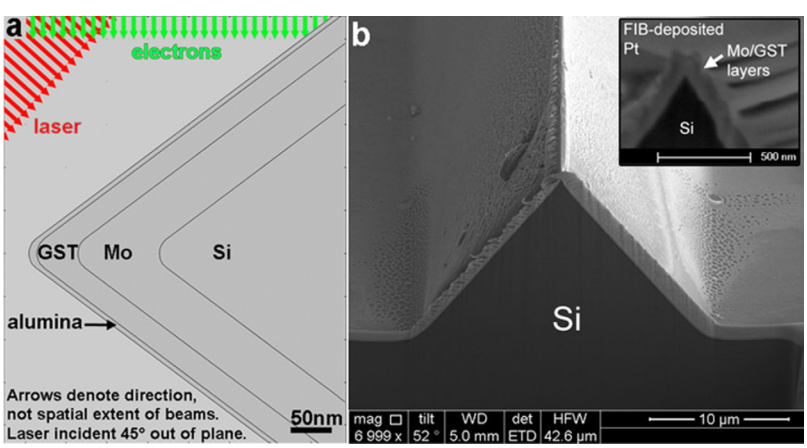

FIG. 2. (Color online) Specimen designed for *in situ* switching shown in (a) schematic and (b) SEM after sectioning with a focused ion beam. $Ge_2Sb_2Te_5$ (GST) at the wedge tip is electron transparent.

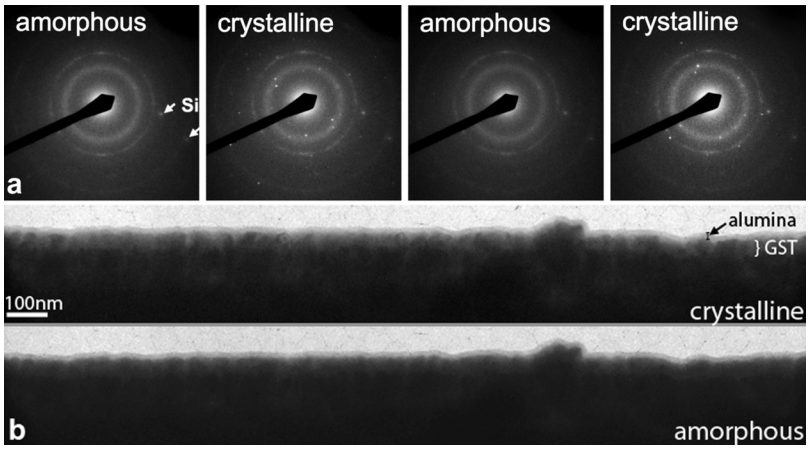

FIG. 3. (a) Two cycles of *in situ* switching and (b) area used to generate the diffraction patterns after a crystallizing pulse (top) and an amorphizing pulse (bottom).

IV. FINITE ELEMENT ANAYLSIS MODELING

The interaction of light with composite materials with complicated geometries can be highly complex. It is also experimentally challenging to measure temperature in nanostructured materials during *in situ* experiments especially when very large spatial and temporal temperature gradients exist. To help understand the *in situ* experiments, the interactions were simulated in a commercial finite element package, COMSOL™. Laser-specimen interactions, including specimen geometry and materials properties as well as wavelength and polarization of the incident laser, were modeled in a time-harmonic study. The incident light was taken to be a uniform plane wave incident at 45°, which is a good approximation because the spot size in the experiment was much larger than the area of interest. This plane wave served as the source term in a standard scattered-wave electrodynamics calculation. The simulation region was bounded by perfectly matched layers that implemented the boundary condition that no waves apart from the specified source term were inbound from outside the region. To save on computational time, a 2D model was used, and the Si wedge and block were truncated relative to the experimental set-up as shown in Fig. 4 (cf. Fig. 2(b)). The model dimensions are large enough that changes in the dimension do not significantly affect the absorption and temperature profiles in the area of interest around the tip of the wedge. The Mo layer was wrapped around the Si block to prevent edge effects, which in this case would otherwise cause spurious intensity at the Mo-Si interface. The absorption is seen in Fig. 5 to be highly inhomogeneous. The results of the laser-specimen interaction simulation were fed directly into a heat transport simulation. For the heat transport simulation, the absorption was given a time-dependent envelope reflecting the temporal profile of the DTEM pump laser (Gaussian pulse centered at 15 ns, 12-ns FWHM) forming a heat source. It was assumed that heat diffusion through the solid is the most significant path for heat flow; radiative losses were ignored. In modeling the amorphization process, the magnitude of the heat source was scaled such that the peak temperature at the tip of the wedge (the electron transparent part) exceeded the melting temperature of $Ge_2Sb_2Te_5$. The simulation was evaluated at 1-ns increments. A plot of the temperature versus time for the $Ge_2Sb_2Te_5$ at the tip of the wedge is shown in Fig. 6(a). The peak temperature occurs at 19 ns, a few ns after the peak intensity of the pump laser. At 40 ns, just 21 ns after the peak temperature, the tip is below T_c, which has been experimentally determined as 415 K^4 though it varies with heating

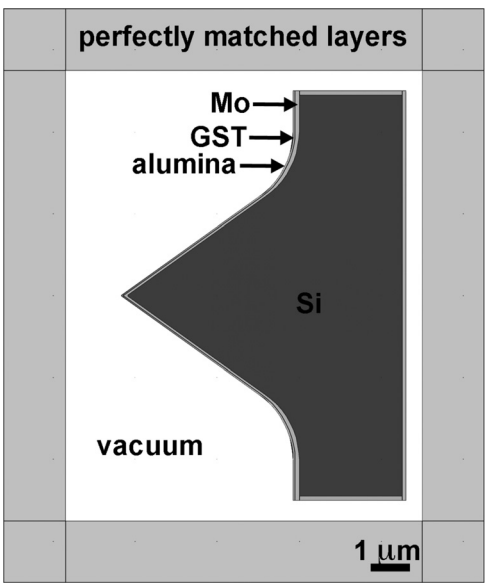

FIG. 4. Overview of the model used for finite element analysis. The Mo wraps around the Si.

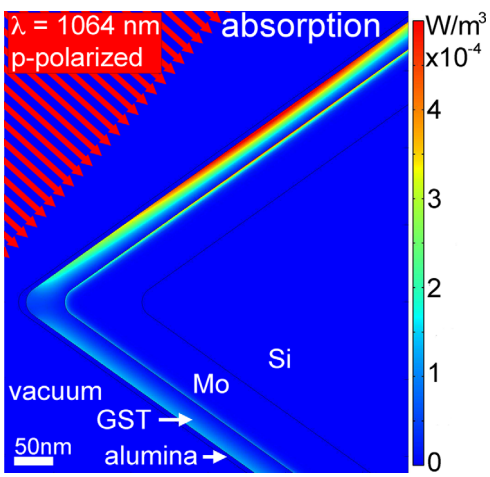

FIG. 5. (Color online) Time-independent absorption profile.

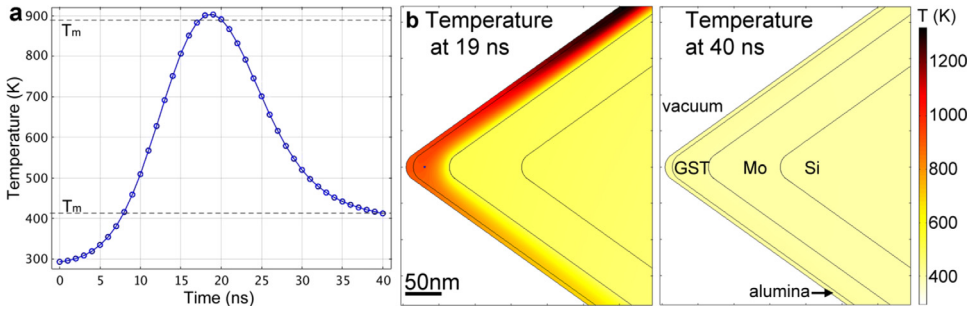

FIG. 6. (Color online) (a) Temperature profile vs time for a point in the GST at the tip of the wedge, marked by a blue dot in (b). (b) Temperature profile at 19 and 40 ns. At 19 ns, the maximum temperature is reached and the electron transparent region exceeds the $Ge_2Sb_2Te_5$ (GST) melting temperature.

rate and will be higher for faster rates.[20] The spatial profiles of the temperature for two times are shown in Fig. 6(b); very large spatial temperature gradients exist when the specimen is at the peak temperature at 19 ns.

The absorption profile simulation does not include changes in material properties due to temperature changes or phase transformations. Because amorphous $Ge_2Sb_2Te_5$ has a substantially lower absorption coefficient than the rock salt phase in the near infrared portion of the spectrum,[23] the absorption of heat should rapidly decrease once the material starts to melt. The simulation also neglects the heat of fusion, which will be absorbed during melting but not released again until much later, during crystallization of the amorphous material. Thus the simulation should slightly underestimate the quench rate because unlike in the simulation, the real $Ge_2Sb_2Te_5$ will not increase significantly in temperature once the melting point is reached. In spite of this, the model captured the speed with which the cooling must occur for the amorphous state to be quenched in. The quench rate predicted from the time to go from the peak temperature to below the T_c is $\sim 10^{10}$ K/s, which is in the range of quench rates reportedly needed to achieve amorphization.[3,4]

While detailed validation of the calculated spatiotemporal temperature profiles is currently not possible, the calculations do predict peak temperatures and cooling rates for a given sample geometry and laser parameters. These predictions can be tested against the experiments, for the observed transformations can only occur above certain known temperatures and cooling rates. Our initial success in matching the experimental observables is promising, indicating such models can guide design and interpretation of nanostructures for future experiments involving high temperature gradients and rapidly driven phase transformations.

V. SUMMARY

Here we have used the DTEM to follow the crystallographic changes in rapidly driven laser induced phase transformations in $Ge_2Sb_2Te_5$ on the nanosecond time scale. We found that crystallization nears completion in about 2 μs; the long crystallization time is due to low cooling rates in large thin, electron-transparent specimens. Specimen geometry has been optimized for the examination of phase transformations that require quench rates on the order of 10^{10} K/s. These quench rates were achieved during *in situ* TEM as shown by successful amorphization of $Ge_2Sb_2Te_2$. These temporal temperature profiles have been successfully modeled using finite element analysis. The finite element analysis is a powerful tool for the interpretation of *in situ* experiments, where accurate methods for measuring rapidly changing temperature profiles are not available and may be anticipated to be of widespread importance in advancing the understanding of *in situ* experiments in the future.

ACKNOWLEDGMENTS

This work was performed under the auspices of the U.S. Department of Energy by Lawrence Livermore National Laboratory under Contract DE-AC52-07NA27344. The Office of Basic Energy Sciences, Division of Materials Sciences and Engineering funded M.K.S., T.L., and G.H.C. The Laboratory Directed Research and Development Program at LLNL funded B.W.R. and N.D.B. under project 08-ERD-032. We thank A. Minor for providing the etched Si wedges, N. Teslich for FIB, and F. Hayes for assistance with the SEM at UCD.

[1]S. Raoux and M. Wuttig, *Phase Change Materials: Science and Applications* (Springer Verlag, Berlin, 2008).
[2]V. Weidenhof, I. Friedrich, S. Ziegler, and M. Wuttig, J. Appl. Phys. **89**, 3168 (2001).
[3]V. Weidenhof, N. Pirch, I. Friedrich, S. Ziegler, and M. Wuttig, J. Appl. Phys. **88**, 657 (2000).
[4]N. Yamada, E. Ohno, K. Nishiuchi, N. Akahira, and M. Takao, J. Appl. Phys. **69**, 2849 (1991).
[5]W. J. Wang, L. P. Shi, R. Zhao, K. G. Lim, H. K. Lee, T. C. Chong, and Y. H. Wu, Appl. Phys. Lett. **93**, 043121 (2008).
[6]R. M. Shelby and S. Raoux, J. Appl. Phys. **105**, 104902 (2009).
[7]S. Raoux, J. L. Jordan-Sweet, and A. J. Kellock, J. Appl. Phys. **103**, 114310 (2008).
[8]Y. Tanaka, Y. Fukuyama, N. Yasuda, J. Kim, H. Murayama, S. Kohara, H. Osawa, T. Nakagawa, S. Kimura, K. Kato, F. Yoshida, H. Kamioka, Y. Moritomo, T. Matsunaga, R. Kojima, N. Yamada, K. Toriumi, T. Ohshima, H. Tanaka, and M. Takata, Jap. J. Appl. Phys. **48**, 03A001 (2009).
[9]G. Ruitenberg, A. K. Petford-Long, and R. C. Doole, J. Appl. Phys. **92**, 3116 (2002).
[10]S. A. Song, W. Zhang, H. S. Jeong, J. G. Kim, and Y. J. Kim, Ultramicroscopy **108**, 1408 (2008).
[11]M. H. Kwon, B. S. Lee, S. N. Bogle, L. N. Nittala, S. G. Bishop, J. R. Abelson, S. Raoux, B. K. Cheong, and K. B. Kim, Appl. Phys. Lett. **90**, 021923 (2007).
[12]Y. W. Jung, S. W. Nam, and R. Agarwal, Nano Lett. **11**, 1364 (2011).
[13]B. S. Lee, G. W. Burr, R. M. Shelby, S. Raoux, C. T. Rettner, S. N. Bogle, K. Darmawikarta, S. G. Bishop, and J. R. Abelson, Science **326**, 980 (2009).
[14]M. Naito, M. Ishimaru, Y. Hirotsu, R. Kojima, and N. Yamada, J. Appl. Phys. **107**, 103507 (2010).
[15]M. R. Armstrong, K. Boyden, N. D. Browning, G. H. Campbell, J. D. Colvin, W. J. DeHope, A. M. Frank, D. J. Gibson, F. Hartemann, J. S. Kim,

W. E. King, T. B. LaGrange, B. J. Pyke, B. W. Reed, R. M. Shuttlesworth, B. C. Stuart, and B. R. Torralva, Ultramicroscopy **107**, 356 (2007).
[16]B. W. Reed, M. R. Armstrong, N. D. Browning, G. H. Campbell, J. E. Evans, T. LaGrange, and D. J. Masiel, Microsc. Microanal. **15**, 272 (2009).
[17]T. LaGrange, G. H. Campbell, P. E. A. Turchi, and W. E. King, Acta Mater. **55**, 5211 (2007).
[18]J. S. Kim, T. LaGrange, B. W. Reed, M. L. Taheri, M. R. Armstrong, W. E. King, N. D. Browning, and G. H. Campbell, Science **321**, 1472 (2008).
[19]L. Nikolova, T. LaGrange, B. W. Reed, M. J. Stern, N. D. Browning, G. H. Campbell, J. C. Kieffer, B. J. Siwick, and F. Rosei, Appl. Phys. Lett. **97**, 203102 (2010).
[20]S. Raoux, Annu. Rev. Mater. Res. **39**, 25 (2009).
[21]A. Minor, dissertation thesis, University of California, 2002.
[22]A. M. Minor, E. T. Lilleodden, E. A. Stach, and J. W. Morris, J. Electron. Mater. **31**, 958 (2002).
[23]B. S. Lee, J. R. Abelson, S. G. Bishop, D. H. Kang, B. K. Cheong, and K. B. Kim, J. Appl. Phys. **97**, 093509 (2005).